

*promoting access to White Rose research papers*



**Universities of Leeds, Sheffield and York**  
**<http://eprints.whiterose.ac.uk/>**

---

This is an author produced version of a paper published in **Continental Shelf Research**

White Rose Research Online URL for this paper:

<http://eprints.whiterose.ac.uk/id/eprint/77687>

---


**Paper:**

O'Hara Murray, RB, Hodgson, DM and Thorne, PD (2012) *Wave groups and sediment resuspension processes over evolving sandy bedforms*. Continental Shelf Research, 46. 16 - 30. ISSN 0278-4343

<http://dx.doi.org/10.1016/j.csr.2012.02.011>

---

## AUTHOR QUERY FORM

|  |  |  |
|--|--|--|
| <br><b>ELSEVIER</b> | <b>Journal: CSR</b><br><br><b>Article Number: 2522</b> | <b>Please e-mail or fax your responses and any corrections to:</b><br><br><b>E-mail: <a href="mailto:corrections.esch@elsevier.macipd.com">corrections.esch@elsevier.macipd.com</a></b><br><br><b>Fax: +44 1392 285878</b> |
|--|--|--|

Dear Author,

Please check your proof carefully and mark all corrections at the appropriate place in the proof (e.g., by using on-screen annotation in the PDF file) or compile them in a separate list. Note: if you opt to annotate the file with software other than Adobe Reader then please also highlight the appropriate place in the PDF file. To ensure fast publication of your paper please return your corrections within 48 hours.

For correction or revision of any artwork, please consult <http://www.elsevier.com/artworkinstructions>.

Any queries or remarks that have arisen during the processing of your manuscript are listed below and highlighted by flags in the proof. Click on the [Q](#) link to go to the location in the proof.

| Location in article | Query / Remark: <a href="#">click on the Q link to go</a><br>Please insert your reply or correction at the corresponding line in the proof |
|---------------------|--|
| <a href="#">Q1</a>  | Please confirm that given names and surnames have been identified correctly.   |
| <a href="#">Q2</a>  | Please check the address for the corresponding author that has been added here, and correct if necessary.                                  |
| <a href="#">Q3</a>  | Please check the telephone number and e-mail address of the corresponding author, and correct if necessary.                                |

Thank you for your assistance.

Contents lists available at [SciVerse ScienceDirect](#)

# Continental Shelf Research

journal homepage: [www.elsevier.com/locate/csr](http://www.elsevier.com/locate/csr)

## Highlights

### Wave groups and sediment resuspension processes over evolving sandy bedforms

*Continental Shelf Research* ■ (■■■■) ■■■-■■■Rory B. O'Hara Murray<sup>a,b</sup>, David M. Hodgson<sup>a</sup>, Peter D. Thorne<sup>b</sup><sup>a</sup> School of Environmental Sciences, University of Liverpool, 4 Brownlow Street, Liverpool L69 3GP, UK<sup>b</sup> National Oceanography Centre, 6 Brownlow Street, Liverpool L3 5DA, UK

► Water velocities, bedforms and suspended sediments were monitored beneath irregular waves. ► Wave boundary layer and free stream sediment suspensions under wave groups were examined. ► Sediment suspensions were observed to fluctuate at wave group time scales. ► Initial entrainment within the wave boundary layer was dominated by intra-wave processes. ► Wave group character was deemed to be an important control over free stream sediment suspensions.

Contents lists available at [SciVerse ScienceDirect](http://SciVerse ScienceDirect)

## Continental Shelf Research

journal homepage: [www.elsevier.com/locate/csr](http://www.elsevier.com/locate/csr)

# Wave groups and sediment resuspension processes over evolving sandy bedforms

Rory B. O'Hara Murray<sup>a,b,1,\*</sup>, David M. Hodgson<sup>a</sup>, Peter D. Thorne<sup>b</sup>

<sup>a</sup> School of Environmental Sciences, University of Liverpool, 4 Brownlow Street, Liverpool L69 3GP, UK

<sup>b</sup> National Oceanography Centre, 6 Brownlow Street, Liverpool L3 5DA, UK

## ARTICLE INFO

## Article history:

Received 7 May 2011

Received in revised form

3 February 2012

Accepted 18 February 2012

## Keywords:

Wave pumping

Ripples

Bedforms

Irregular waves

Acoustics

ABS

## ABSTRACT

High resolution measurements of the water velocity, bedforms and suspended sediment concentration were made using an Acoustic Doppler Velocimeter, acoustic bedform scanners and an Acoustic Backscatter System, under irregular free-surface waves. The waves were generated in a large scale flume facility above a number of bedform types. These data were analysed in (i) the frequency domain in order to examine the frequency at which sediment suspensions occurred in the oscillatory bottom boundary layer and the free stream; and (ii) the time domain in order to examine the instantaneous entrainment and vertical transport of sediment at intra-wave, wave average and wave group time scales. During the course of the experiments the significant wave height was systematically incremented enabling the character of sediment suspensions to be studied under a number of flow and bedform regimes. Wave groups were identified as an important control over sediment suspensions in both the wave boundary layer and free stream, with fluctuations in the suspended sediment concentration occurring at low, wave group, frequencies. However, the initial entrainment process, within the wave boundary layer, occurred at intra-wave frequencies. In contrast, in the free stream, sediment suspensions were dominated by the vertical transport of sediment at wave group time scales. During wave groups the sediment suspension field was characterised by the upward transport of sediment due to the continual injection of turbulence under a series of waves which generated a wave pumping effect. The character of a wave group is considered to be an important control over sediment suspensions in the free stream. Four distinct types of wave group were identified and the instantaneous sediment suspension field below each type examined. Such comparisons were possible using the high resolution Acoustic Backscatter System which enabled both intra-wave and wave group processes to be resolved up to 0.8 m above the bed.

© 2012 Elsevier Ltd. All rights reserved.

## 1. Introduction

Under irregular waves, the suspended sediment concentration (SSC) changes over a range of time scales (Hanes, 1991; Osborne and Greenwood, 1993; Hay and Bowen, 1994b; Williams et al., 2002). These fluctuations occur at high, intra-wave, frequencies associated with individual waves (Osborne and Vincent, 1996; Villard and Osborne, 2002; O'Hara Murray et al., 2011) and also at low, infra-gravity, frequencies (Hanes, 1991; Osborne and Greenwood, 1993) associated with wave groups (Clarke et al., 1982; Larsen, 1982; Vincent et al., 1982, 1991; Shi and Larsen, 1984; Hay and Bowen, 1994a). The suspension of sediment is strongly dependent on the hydrodynamics and the type of bedforms present (Vincent et al.,

1991; Ribberink and Al-Salem, 1994; Vincent et al., 1999; Grasmeyer and Kleinhans, 2004). Above steep-sided two-dimensional ripples, flow separation can occur during each wave half-cycle, forming a sediment-laden vortex, which at flow reversal is ejected out of the wave boundary layer (WBL) and into the free stream (Nakato et al., 1977; Hansen et al., 1994; Sleath and Wallbridge, 2002). In these conditions, the intra-wave suspension of sediment is a convective entrainment process occurring twice in a wave cycle (Davies and Thorne, 2005; Van der Werf et al., 2007; Thorne et al., 2009). When the bed is plane the entrainment of sediment occurs when the peaks in the bed shear stress generate turbulence, which occurs just ahead of peak free stream velocity (Davies and Thorne, 2008), and is a diffusive process. These intra-wave entrainment processes are strongly dependent on the properties of each incident wave—its height, period and asymmetry. During the passage of a group of waves, however, the SSC also depends on the properties of antecedent waves. For example, at a given height above the bed the SSC is often higher under waves later in a group than under similar waves early in a wave group (Hanes, 1991; Villard et al., 2000; Vincent and Hanes, 2002). This can be due

\* Corresponding author at: School of Environmental Sciences, University of Liverpool, 4 Brownlow Street, Liverpool L69 3GP, UK. Tel.: +44 151 7945150.

E-mail addresses: [r.murray@marlab.ac.uk](mailto:r.murray@marlab.ac.uk), [roryohm@gmail.com](mailto:roryohm@gmail.com) (R.B. O'Hara Murray).

<sup>1</sup> Current address: Marine Scotland Science, Marine Laboratory, P.O. Box 101, 375 Victoria Road, Aberdeen AB11 9DB, UK

to the process of wavepumping, where within each wave cycle sediment is entrained to increasingly higher elevations before it can settle. The continual injection of turbulence under consecutive waves in a wave group leads to more sediment being supported, and to the vertical advection of turbulence during the passage of a wave group (Osborne and Greenwood, 1993). A consequence of the wave pumping process is a time lag between the initial entrainment of sediment at the bed and higher than average concentrations at high elevations in the free stream (Vincent and Hanes, 2002).

This work uses high frequency acoustic technology to examine time series of SSC up to 0.8 m above a number of different bedform types that developed in a large scale wave flume as the significant wave height was systematically incremented. In addition to the SSC, the water velocities and the bedform dimensions and geometries were measured using acoustics. Over a variety of bedforms, the fluctuations in SSC within the WBL are considered to be associated with intra-wave entrainment processes, while in the free stream the SSC variation is deemed to be a function of the wave group and is dependent on antecedent waves. This is because the vertical extent to which the intra-wave processes dominate is often limited by the ripple height (Van Rijn, 1993; Van der Werf et al., 2006; Thorne et al., 2009), whereas the process of wave pumping can entrain sediment high into the free stream. This work aims to examine the temporal differences between sediment resuspension in the WBL and free stream under wave groups. Wave groups are characteristic of irregular free surface waves typical of field conditions. The importance of considering wave groups when trying to understand sediment entrainment and transport processes is highlighted, and raises the question of how important the character of the wave group is, such as the number of waves and distribution of wave heights in a group. Finally, a number of future research avenues and experimental refinements are suggested.

## 2. Experiments, instrumentation and data analysis

The Deltaflume of Deltares Delft Hydraulics, the Netherlands, is a large scale flume (240 m long, 5 m wide and 7 m deep) that enables sediment transport processes to be monitored at field scale. Irregular waves with a JONSWAP spectrum (Carter, 1982) were generated for a series of significant wave heights during which the bed adopted a number of different morphological forms. A series of experiments was conducted over an upper-medium-grained sand bed in water

depths of approximately 4 m. The 11 experiments are here referred to as M01–M11. Twelve samples of the bed sediments were taken from a variety of locations on the bed and their volume size distributions were determined using a Coulter Laser Granulometer. The bed sediments were found to have a lognormal grain size distribution with a median grain diameter,  $D_{50}$ , of  $375 \pm 30 \mu\text{m}$ . The bed was 0.7 m deep and was laid down in the centre of the flume in a 30 m long region spanning the width of the flume. Prior to the 25 min measurement burst of each experiment, the irregular waves were run for one hour to allow the bedforms to reach equilibrium (Marsh et al., 1999) and for any air trapped in the bed sediments to degas. Fig. 1 is a schematic of the instruments deployed on a frame mid-way along the sandy bed and at one side of the Deltaflume. The Nortek Vector Acoustic Doppler Velocimeter (ADV) measured the water velocities at one point  $\sim 0.5$  m above the bed and recorded the three components of flow at 16 Hz. The cross-shore cross-sectional and plan-form geometry of the bedforms were monitored by a 2.0 MHz Acoustic Ripple Profiler (ARP) and 1.2 MHz Sector Scanning Sonar (SSS), respectively. Vertical profiles of the suspended sediment concentration, at 4 Hz intra-wave time scales, were measured by an Acoustic Backscatter System (ABS). The ABS comprised three transceivers operating at 1.0, 2.0 and 4.0 MHz, aligned along-shore and perpendicular to the oscillatory flow. Finally, pumped samples of the suspended sediments (Bosman et al., 1987) were taken from up to five heights above the bed during M03–M11. These samples were analysed using laser granulometry to obtain grain size distributions of the suspended sediment.

In the experimental study, measurements of the wave forcing, bedforms and suspended sediment concentration were made. Wave generated bedforms quickly emerged, and, as the significant wave height was incremented, exhibited a number of different plan-form and cross-sectional configurations. Thus, measurements of the SSC were made above an evolving sandy bed and the response of the SSC during the passage of wave groups, and over different bedforms, was examined.

### 2.1. Irregular wave forcing and wave groups

For each experiment, the ADV velocity components were despiked using a Phase-Space Thresholding Method (Goring and Nikora, 2002) and rotated to correct for any misalignment of the instruments with the main flow direction by calculating the principle axis of variation (Emery and Thompson, 1997). During

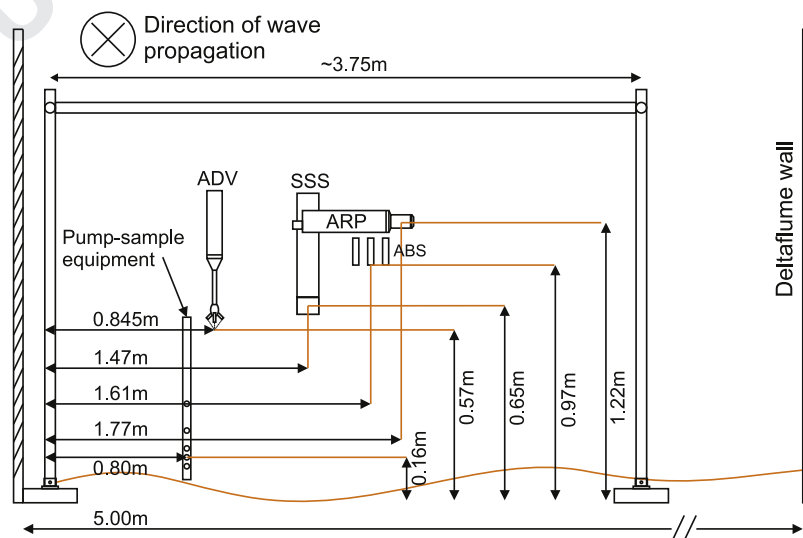


Fig. 1. A schematic of the instruments deployed on a frame in the Deltaflume showing the locations of the Acoustic Doppler Velocimeter (ADV), Acoustic Ripple Profiler (ARP), Sector Scanning Sonar (SSS), Acoustic Backscatter System (ABS) and pump sampling equipment.

the series of experiments the significant wave height was systematically incremented, while the peak spectral wave period,  $T_p$ , was kept constant at 6.1 s. Therefore, the surface wave steepness increased with the significant wave height. The significant wave height,  $H_s$ , was calculated for each experiment from the power spectral density (PSD) of the horizontal cross-shore velocity component from the ADV using (Wiberg and Sherwood, 2008)

$$H_s = 4 \sqrt{\sum_i^N \frac{S_i \Delta f_i}{[2\pi f_i \cosh(k_i z_A) / \sinh(k_i h)]^2}} \quad (1)$$

where  $S_i$  and  $k_i$  are the power spectral density and wavenumber, respectively, at the frequency  $f_i$ ,  $z_A$  is the height of the ADV above the bed,  $h$  is the mean water depth,  $\Delta f_i = f_{i+1} - f_i$  and  $N$  is the number of frequency intervals within the range  $0.1 \leq f \leq 0.4$  Hz. This frequency interval was chosen in order to exclude high frequency contributions due to turbulence, and low frequency contributions associated with wave groups. In a similar manner, the significant orbital velocity,  $U_s$ , was calculated using Wiberg and Sherwood (2008)

$$U_s = \sqrt{4 \sum_i^N S_i \Delta f_i} \quad (2)$$

The  $H_s$  and  $U_s$  results from the Deltaflume experiments are listed in Table 1 along with the significant orbital diameter given by  $d_s = U_s T_p / \pi$ , with  $T_p = 6.1$  s, and the grain roughness Shields parameter given by

$$\theta_{2.5} = \frac{f_{2.5} U_s^2}{2(s-1)gD_{50}} \quad (3)$$

In Eq. (3),  $s$  is the ratio of sediment density to water density ( $s = 2.65$  for the quartz sand used),  $g$  is the acceleration due to gravity and  $f_{2.5}$  is the grain roughness wave friction factor (skin friction) based on the equivalent Nikuradse grain roughness,  $2.5D_{50}$ , calculated using the formula of Soulsby (1997).

Fig. 2(a) shows extracts of the horizontal cross-shore velocity time series from the ADV for M03, M06 and M09 during which  $H_s$  was 0.53, 1.05 and 1.63 m, respectively. The systematic increase in velocity amplitudes with  $H_s$  is clearly observed in Fig. 2(a). One feature in Fig. 2(a) is the presence of wave groups during each experiment, with two or more wave cycles, typically 6–10, growing then shrinking in velocity amplitude. Fig. 2(a) also shows that the timing of the wave groups is consistent across the experiments. This is because the JONSWAP algorithm used by the wave paddle differed only by the significant wave height for each experiment. Fig. 2(b) shows the PSD of 25 min bursts of cross-shore velocity, from the same experiments shown in Fig. 2(a). These spectra were obtained by performing a Fast Fourier Transform on the velocity time series. The efficiency of this transformation was increased by zero padding

the velocity time series to a length equal to  $2^{15}$ . A Hamming window was applied over the length of the time series (Emery and Thompson, 1997) and band averaging was performed over 16 discrete frequency samples, giving 32 degrees of freedom to each of the final 1024 frequency bands of the single-sided spectra. The 99% confidence interval was calculated using the chi-square approach and is indicated in the figure. The major peak between 0.1 and 0.4 Hz in Fig. 2(b) corresponds to oscillations at the wave frequency and is broad because the waves were irregular. The significant wave heights were calculated using only this part of the spectra. Above 0.4 Hz, the spectra are dominated by turbulence. Below 0.1 Hz there are three statistically significant peaks in the spectra, considered to be associated with the wave groups.

## 2.2. Bedforms

The ARP scanned a 4 m cross-shore transect of the bed approximately once in a minute at centimetre horizontal resolution and sub-centimetre vertical resolution providing cross-sections of the bed. Fig. 3(a) shows the ARP bedform cross-sections from the Deltaflume experiments, during which  $H_s$  was increased. Each result shows approximately 10 min worth of data out of the 25 min bursts. The associated SSS results were rectified from polar to square grid coordinates (Bell and Williams, 2002) to give  $5 \times 5$  m images of the bed, enabling the plan-form geometry of the bedforms to be studied. Fig. 3(b)–(f) shows a selection of these results depicting the different ripple plan-form configurations that emerged as  $H_s$  was increased. The plan-form geometries of the ripples during each experiment were classified using the terminology of Pedocchi and Garcia (2009), who described ripples as either two-dimensional (2D), quasi-two-dimensional (q-2D) or three-dimensional (3D). These plan-form ripple geometries were observed during the Deltaflume experiments and their occurrence is indicated in Fig. 3(a). Whilst  $H_s = 0.34$ – $0.64$  m (M01–M04) the ripples were 2D. As  $H_s$  increased through 0.85 and 1.05 m (M05, M06) the ripples became q-2D, and then 3D when  $H_s = 1.29$  and 1.50 m (M07, M08). When  $H_s$  was further increased to 1.63–1.70 m (M09–M11) the 3D ripples became much larger and resembled lunate mega-ripples (Vincent and Osborne, 1993; Vincent et al., 1999) or hummocks (Green and Black, 1999). The plan-form geometry classifications for each experiment are listed in Table 1.

A turning point analysis was used to extract the nominal dimensions of the ripples during each experiment from the ARP cross-sections. A low pass Gaussian filter removed high frequency spatial fluctuations and a running average smoothed spikes due to sediment resuspension under large waves. Ripple wavelengths were taken as the horizontal distances between adjacent troughs either side of a crest, ripple heights were taken as the mean average crest to trough difference either side of the crests and the ripple steepness were taken as the height-to-length ratios. The

**Table 1**  
Experimental parameters and bedform conditions for the irregular wave Deltaflume experiments.

| Exp. | $H_s$ (m) | $U_s$ (m/s) | $d_s$ (m) | $\theta_{2.5}$ | $k_s$ (m) | $\delta_w$ (m) | $\lambda$ (m) | $\eta$ (m) | $\eta/\lambda$ | Plan-form bedform geometry |
|------|-----------|-------------|-----------|----------------|-----------|----------------|---------------|------------|----------------|----------------------------|
| M01  | 0.34      | 0.22        | 0.42      | 0.054          | 0.005     | 0.029          | 0.227         | 0.004      | 0.017          | 2D                         |
| M02  | 0.43      | 0.28        | 0.54      | 0.079          | 0.016     | 0.047          | 0.145         | 0.010      | 0.067          | 2D                         |
| M03  | 0.53      | 0.34        | 0.66      | 0.107          | 0.035     | 0.067          | 0.211         | 0.024      | 0.105          | 2D                         |
| M04  | 0.64      | 0.40        | 0.78      | 0.138          | 0.042     | 0.080          | 0.224         | 0.026      | 0.109          | 2D                         |
| M05  | 0.85      | 0.53        | 1.04      | 0.209          | 0.048     | 0.102          | 0.289         | 0.029      | 0.099          | q-2D                       |
| M06  | 1.05      | 0.66        | 1.28      | 0.285          | 0.055     | 0.123          | 0.350         | 0.032      | 0.093          | q-2D                       |
| M07  | 1.29      | 0.79        | 1.54      | 0.374          | 0.067     | 0.149          | 0.536         | 0.045      | 0.086          | 3D                         |
| M08  | 1.50      | 0.92        | 1.80      | 0.470          | 0.081     | 0.175          | 0.609         | 0.056      | 0.088          | 3D                         |
| M09  | 1.63      | 1.00        | 1.95      | 0.529          | 0.107     | 0.199          | 0.747         | 0.074      | 0.107          | Hummocks                   |
| M10  | 1.70      | 1.03        | 1.99      | 0.548          | 0.096     | 0.197          | 0.975         | 0.084      | 0.076          | Hummocks                   |
| M11  | 1.63      | 0.98        | 1.91      | 0.514          | 0.085     | 0.186          | 0.960         | 0.070      | 0.075          | Hummocks                   |



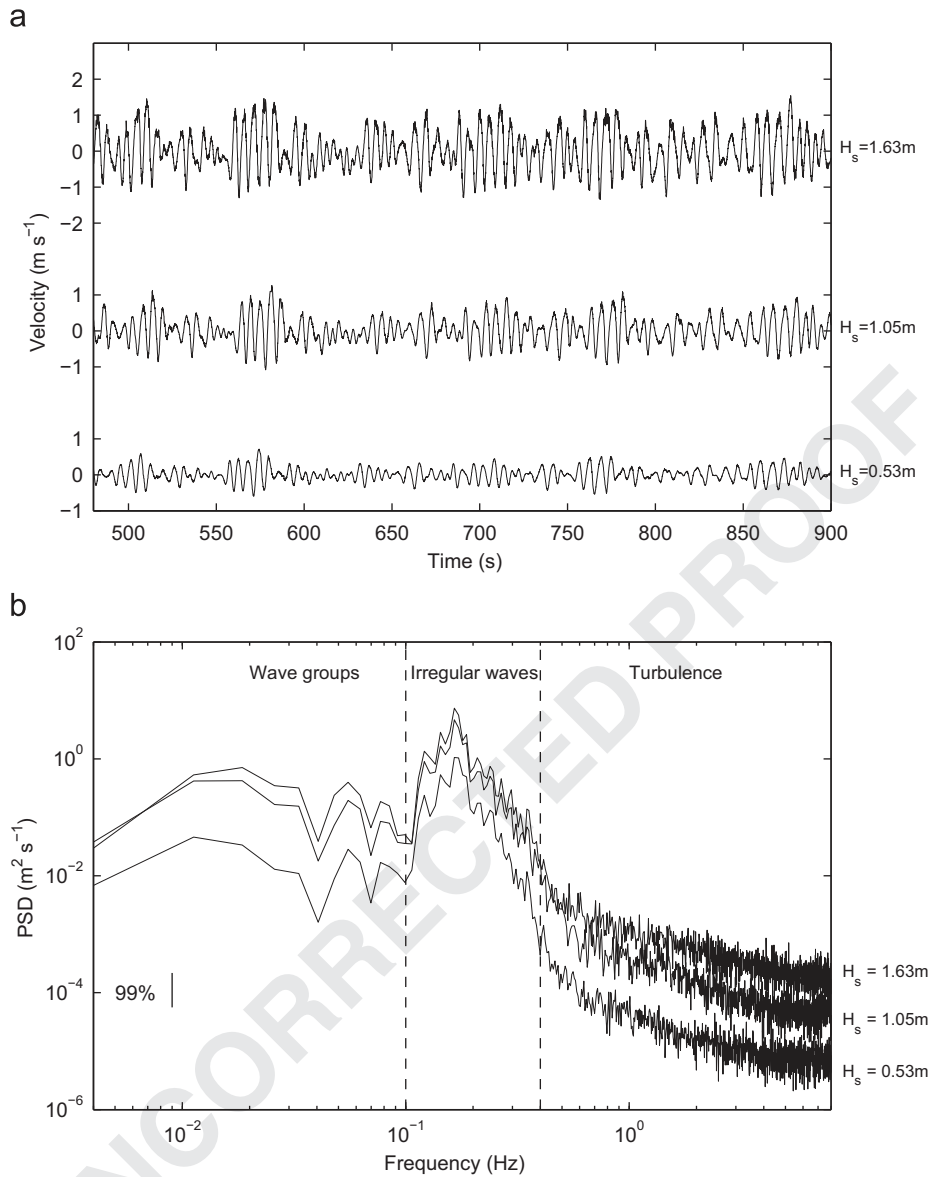


**Fig. 2.** Example results from the cross-shore velocity recorded by the ADV. (a) Time series extracts from three experiments (M03, M06, M09) where the significant wave height,  $H_s$ , was 0.53, 1.05 and 1.63 m. (b) The power spectral density, PSD, from the same three experiments as in (a) with the 99% confidence interval shown and vertical dashed lines showing the irregular wave frequency range, 0.1–0.4 Hz.

average ripple wavelengths,  $\lambda$ , heights,  $\eta$ , and steepness,  $\eta/\lambda$ , are listed in Table 1 for each experiment.

### 2.3. Wave boundary layer

Estimates of the temporally averaged WBL thickness,  $\delta_w$ , during each rippled bed experiment were made using the definition given by Davies and Villaret (1999) with the wave period replaced by the peak spectral period,  $T_p$

$$\delta_w = 5 \sqrt{\frac{K_0 T_p}{2\pi}} \quad (4)$$

In Eq. (4),  $\frac{1}{2}K_0$  is the cycle-mean eddy viscosity estimated using the formula of Nielsen (1992)

$$\frac{K_0}{2} = 0.00253 U_s k_s \sqrt{d_s / 2k_s} \quad (5)$$

with the orbital velocity amplitude and orbital diameter replaced by the significant values,  $U_s$  and  $d_s$ , and where  $k_s$  is the bed

roughness given by Nielsen (1992)

$$k_s = 8\eta \eta / \lambda + 170 D_{50} \sqrt{\theta_{2.5} - 0.05}. \quad (6)$$

The estimated bed roughness and typical WBL thickness for each rippled bed experiment are listed in Table 1. During the experiments  $\delta_w$  increased from  $\sim 2.9$  cm, when the wave forcing was low, to  $\sim 19.9$  cm, at the maximum in the wave forcing. These values of  $\delta_w$ , based on  $H_s$ , are estimates of the temporally averaged WBL thickness for each experiment. The instantaneous thickness of the WBL were expected to fluctuate at wave group frequencies.

### 2.4. Suspended sediments

The ABS measured vertical profiles of backscatter amplitude at a temporal resolution of 128 Hz. The variability in the backscatter signal, due to the random phasing of the acoustic returns (Thorne et al., 1993), was significantly reduced by averaging over 32 independent measurements of the backscatter. This reduced the

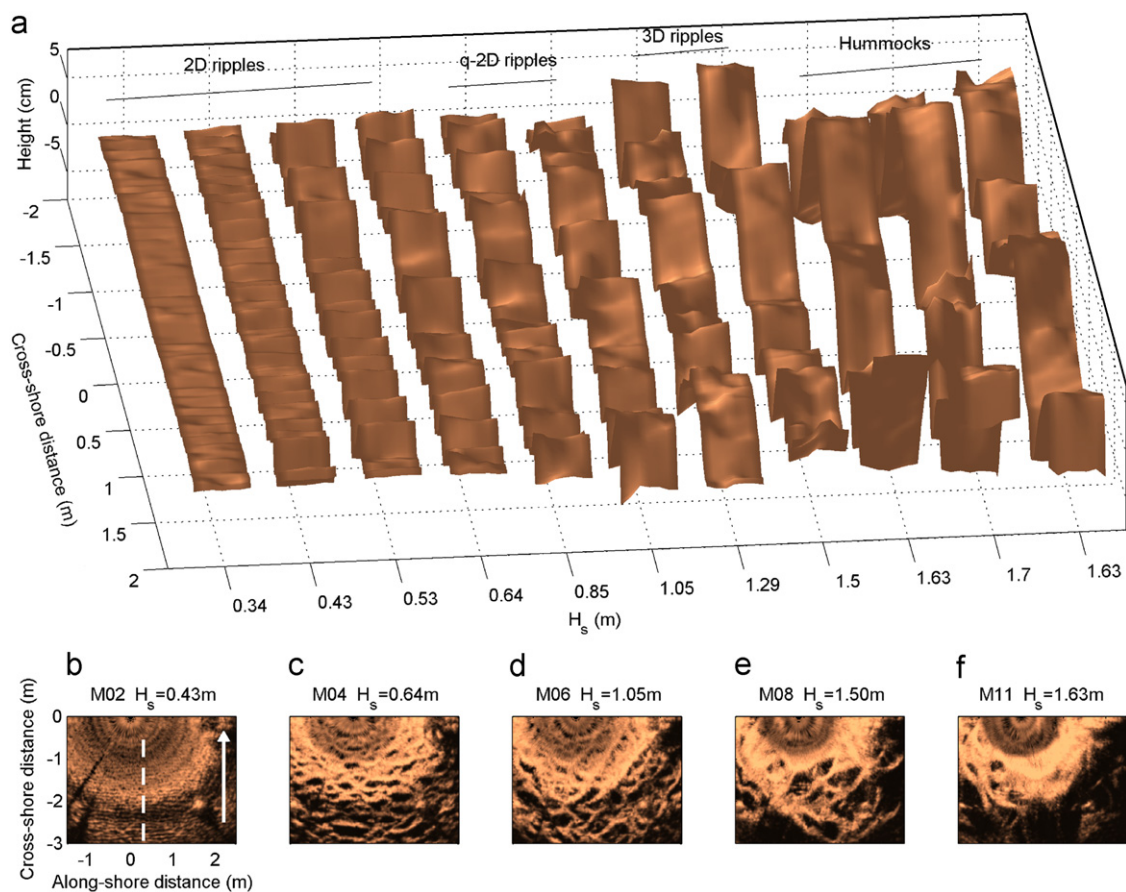


**Fig. 3.** (a) Acoustic ripple profiler cross-sections and (b)–(f) sector scanning sonar plan-form images, depicting the response of the sandy bed to step changes in the significant wave height,  $H_s$ . In (a) the plan-form geometry classifications given are indicated as either 2D, q-2D, 3D or hummocky. In (b) the direction of wave propagation ( $\rightarrow$ ) and the ARP transect line (---) is indicated.

backscatter signal from 128 Hz to 4 Hz, and the standard error by a factor of  $\sqrt{32}$  (Thorne and Hanes, 2002). This was deemed to be an appropriate reduction in the error to distinguish individual stochastic events, while still maintaining a high intra-wave sample rate.

The 4 Hz, 25 min time series, backscatter profiles were converted to instantaneous SSC profiles at 4 Hz using a semi-analytical acoustic inversion, commonly referred to as an implicit inversion (Thorne and Hanes, 2002). These acoustic inversions were aided by measurements of the suspended sediment size distributions obtained from pumped samples of the sediment-laden water as described by O'Hara Murray et al. (2011), which confirmed the veracity of this inversion methodology. The bed level directly below the ABS was tracked during each ABS time series through an examination of the near bed backscattered intensity received by each transceiver. There were small variations in the nominal bed level due to large entrainment events under the more energetic waves and changes in the ripple heights over time (Doucette and O'Donoghue, 2006).

#### 2.4.1. Burst average suspended sediment concentration profiles

Fig. 4 shows five time-mean SSC profiles obtained from experiments M02, M04, M06, M08 and M11 where  $H_s$  ranged from 0.43 to 1.63 m. As  $H_s$  was incremented the plan-form bed morphology evolved from having (M02  $\square$ ) 2D ripples of low steepness, (M04  $\circ$ ) steep-sided 2D ripples, (M06  $+$ ) q-2D ripples, (M08  $\bullet$ ) 3D ripples to (M11  $\times$ ) lunate mega-ripples or hummocks. For  $z > 0.05$  m there

is a clear increase in the magnitude of the SSC profiles with  $H_s$ . This trend breaks down closer to the bed,  $z < 0.05$  m, with the SSC remaining at approximately  $2 \text{ kg m}^{-3}$  for  $H_s > 1$  m. This change in the relationship between  $H_s$  and SSC magnitude, close to the bed, is most likely connected with the transition from 2D to 3D plan-form bedform morphology at the higher wave forcing conditions of  $H_s > 1$  m.

The time-mean SSC profiles shown in Fig. 4 are exponential in form close to the bed, and can be modelled by

$$C(z) = C_0 e^{-z/L}, \quad (7)$$

where  $C_0$  is the cycle-mean reference concentration at  $z=0$  and  $L$  is the exponential decay length scale of the SSC profile. Fitting Eq. (7) to those profiles shown in Fig. 4 for  $0.01 < z < 0.06$  m gave  $L=0.03, 0.07, 0.06, 0.10$  and  $0.07$  m for M02, M04, M06, M08 and M11, respectively.

#### 2.4.2. Wave cycle averaging the suspended sediment concentration profiles

The timing of each individual wave cycle within a measurement burst was identified from the cross-shore ADV velocity time series. The start of each wave cycle was defined as the time of flow reversal from offshore flow to onshore flow. This was done by applying a rectangular low pass filter, with a frequency cut-off at 1 Hz, in order to remove high frequency turbulent fluctuations, and using a zero-crossing analysis to identify the times of flow reversal. These filtered time series were compared with the



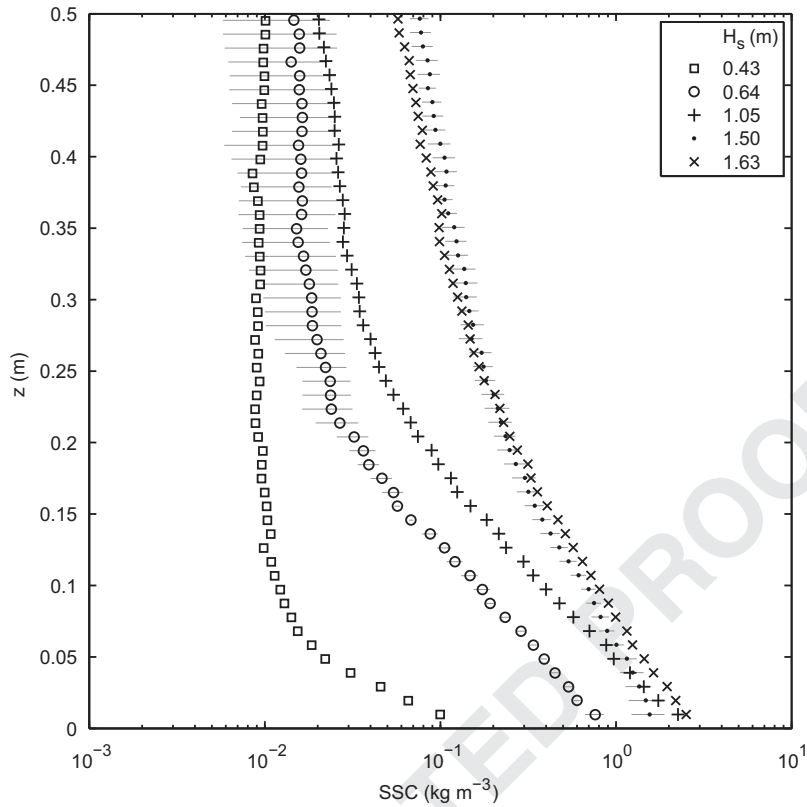


**Fig. 4.** Time-mean suspended sediment concentration, SSC, against height above the bed,  $z$ . These profiles are from experiments M02 ( $\square$ ), M04 ( $\circ$ ), M06 ( $+$ ), M08 ( $\bullet$ ) and M11 ( $\times$ ) during which the significant wave height,  $H_s$ , varied from 0.43 to 1.63 m and different bedforms were present. The results show the mean taken across the results from the three ABS transceivers and the standard error is shown in the cases of M04 and M08 indicating the typical uncertainty in the measurements. The ripple dimensions and plan-form geometries are listed in Table 1.

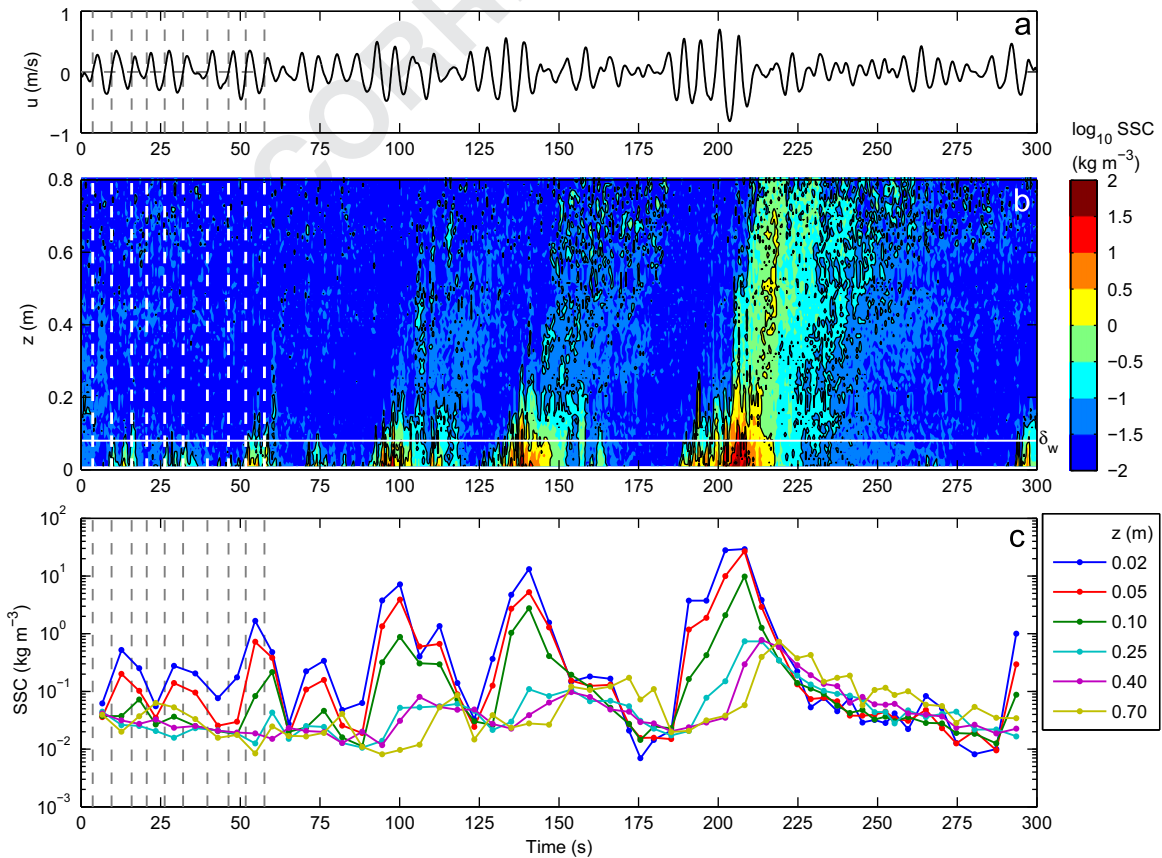


**Fig. 5.** A 5 min time series from M04 of (a) cross-shore velocity,  $u$ , (b) SSC at 2 Hz for  $0 < z < 0.5$  m from the 1 MHz ABS and (c) wave cycle-mean suspended sediment concentration, SSC, at five heights,  $z$ , above the bed from the 1 MHz ABS. The first 10 wave cycles are indicated by the dotted lines in each figure, and in (b) the temporally averaged wave boundary layer thickness,  $\delta_w = 0.080$  m, is indicated by the horizontal white line.

non-filtered time series confirming that the velocities incurred no significant changes in amplitude and phase during the analysis. Having determined the timing of each individual wave cycle in a 25 min measurement burst, cycle-mean profiles of SSC were obtained from the 4 Hz ABS time series of SSC.

Fig. 5 shows a 5 min time series from M04 of (a) cross-shore velocity, (b) instantaneous SSC at 2 Hz up to 0.8 m above the bed and (c) wave cycle-mean SSC at five heights above the bed. The first 10 wave cycles, identified by the zero-crossing analysis of the velocity time series, are indicated by the vertical dashed lines in Fig. 5. Table 1 shows that during M04,  $H_s = 0.64$  m and the ripples were 2D with average steepness of  $\eta/\lambda = 0.11$ . During the time series shown in Fig. 5, the ABS was above a crest of a ripple with a wavelength of 0.33 m, height of 0.047 m and steepness of 0.14 (O'Hara Murray et al., 2011). Fig. 5(b) shows a number of individual peaks in the SSC. These relatively high levels of SSC are individual suspension events, and are generally confined to the near bed region of  $z \leq 0.10$  m and have lifespans of the order of seconds. This near bed region corresponds to  $\delta_w$  which is indicated by the white line in Fig. 5(b). O'Hara Murray et al. (2011) showed that such suspension events occurred consistently just after flow reversal and attributed them to the ejection of sediment-laden vortices over the ripple crest. This vortex shedding process does not occur after every wave half-cycle in Fig. 5, but typically when the orbital diameter is greater than the ripple wavelength (Malarkey and Davies, 2002; O'Hara Murray et al., 2011), and hence they are intermittent through the time series. Whilst Fig. 5(c) does not resolve these intra-wave events, it shows the upward propagation of sediment during wave groups. From Fig. 5(c) it can be seen that at  $z = 0.7$  m the SSC peaks approximately 2–3 wave cycles after the peak at  $z \leq 0.10$  m.

### 3. Results

#### 3.1. The wave pumping effect

Fig. 5(b) shows intermittent sediment suspension events occurring close to the bed,  $z \leq 0.10$  m, at a frequency of one or two times the wave frequency, most likely associated with entrainment by vortices within the WBL. The temporally averaged WBL thickness,  $\delta_w = 0.080$  m, is indicated in Fig. 5(b), but this would have varied during the passage of a wave group with it being thicker under the larger amplitude, and longer period, waves. In addition to the high frequency events within the WBL there are three, lower frequency, suspension events in Fig. 5(b), where sediment is entrained well above the WBL, associated with the passage of wave groups. For example, around 175 s in Fig. 5(a), the orbital velocities were small, with velocity amplitudes of  $\sim 0.07$  m/s, but increased to velocity amplitudes of  $\sim 0.75$  m/s by 200 s. Within the WBL, typically  $z \leq 0.10$  m, the SSC responded quickly to this increase in velocity amplitude, as can be seen in Fig. 5(b) and (c), and started to increase at around 190 s. Above the WBL, typically  $z > 0.10$  m, the SSC was slower to respond and only started to increase around 200 s. Fig. 5(c) shows that the peak in SSC within the WBL occurred at  $\sim 200$ –210 s, whereas farther away from the bed,  $z > 0.20$  m, the SSC peaked at  $\sim 215$ –225 s, 2–3 wave cycles later. This response of the SSC to the passage of a wave group is due to the wave pumping effect (Villard et al., 2000; Vincent and Hanes, 2002), previously observed in the Deltaflume experiments by Williams and Bell (2006). Using the results shown in Fig. 5(c), estimates of the vertical ascent rate of the suspended sediments during the wave group around 200 s were made. During this wave group the SSC peaked at 208.2, 213.6 and 219.1 s, at  $z = 0.02, 0.40$  and  $0.70$  m, respectively.

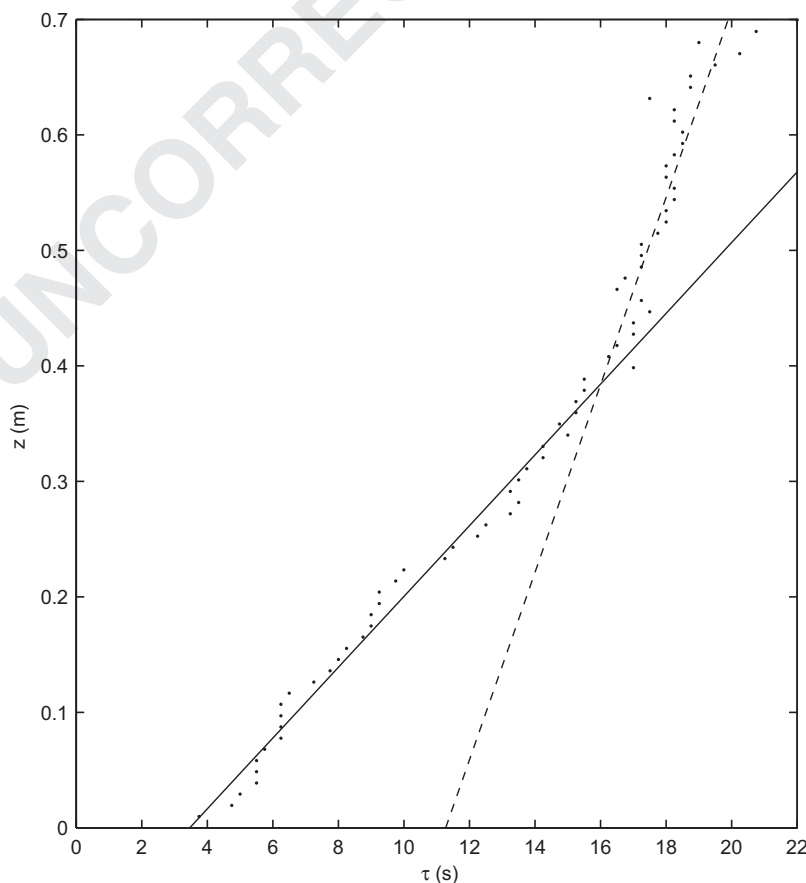


Fig. 6. The variation in the time lag of the maximum in cross-correlation between the SSC and the wave group envelope,  $\tau$ , with height above the bed,  $z$ . The results from regressions made on the data corresponding to  $0 < z < 0.4$  m (—) and  $0.4 < z < 0.7$  m (---) are shown.

From these measurements, three estimates of the vertical ascent rate of the suspended sediment were found to be 0.071, 0.063 and 0.054 m/s, between 0.02–0.40 m, 0.02–0.70 m and 0.40–0.70 m, respectively. This indicates that the vertical ascent rate decreased with height above the bed. Using the formula of Soulsby (1997) the settling velocity of the median bed sediment grain size,  $D_{50} = 375 \mu\text{m}$ , was calculated to be  $w_{s50} = 0.055 \text{ m/s}$ . This analysis indicates that, for  $z < 0.40 \text{ m}$ , the vertical ascent rate of the suspended sediment was greater than  $w_{s50}$ . For  $z > 0.40 \text{ m}$  the ascent rate of 0.054 m/s is equivalent to the settling velocity of grains with a diameter of  $370 \mu\text{m}$ .

The 5 min time series shown in Fig. 5 is part of an approximate 10 min time series during which the ABS was above a ripple crest. A wave group envelope for this 10 min time series was obtained by zero meaning the velocity time series, taking the absolute value and applying a rectangular low pass filter, with a frequency cut-off at 0.05 Hz. A rectangular low pass filter, with the same frequency cut-off, was also applied to the SSC time series. The wave group envelope was re-sampled at the SSC time series sample frequency, 4 Hz, and a cross-correlation was performed between the velocity envelope and the low pass filtered SSC time series, at all heights above the bed. Fig. 6 shows how the time lag between the SSC and velocity envelope at the maximum in cross-correlation,  $\tau$ , varied with height above the bed. There is a clear increase in  $\tau$  with height above the bed, and also a change in

gradient,  $d\tau/dz$ , at  $z \sim 0.4 \text{ m}$ ,  $\tau \sim 16 \text{ s}$ . Fig. 6 also shows the results from regressions made on the data for  $0 < z < 0.4 \text{ m}$  and  $0.4 < z < 0.7 \text{ m}$ , which had correlation coefficients,  $R^2$ , of 0.98 and 0.75, respectively. The gradient,  $d\tau/dz$ , can provide an indication of the vertical ascent rate of the suspended sediment, with  $d\tau/dz = 0$  suggesting that the suspended sediment is not ascending, but moving horizontally with the flow. The change in gradient at  $z \sim 0.4 \text{ m}$  indicates a reduction in the vertical ascent rate, and the lag at this height,  $\tau \sim 16 \text{ s}$ , agrees well with the observation that peak SSC in the free stream occurs 2–3 wave cycles later than in the WBL. Hay and Bowen (1994b) observed a similar cross-correlation in field data during similar wave forcing conditions.

### 3.2. Time scales of sediment entrainment above an evolving bed

The power spectral density (PSD) of the 4 Hz ABS SSC was calculated for each experiment, to further examine the frequencies at which sediment entrainment occurred through the 25 min bursts. The performance of the Fast Fourier Transformation was maximised by zero padding the time series to a length equal to  $2^{13}$ . A Hamming window was applied over the length of the time series (Emery and Thompson, 1997) and band averaging was performed over 32 discrete frequency samples, giving each of the final 128

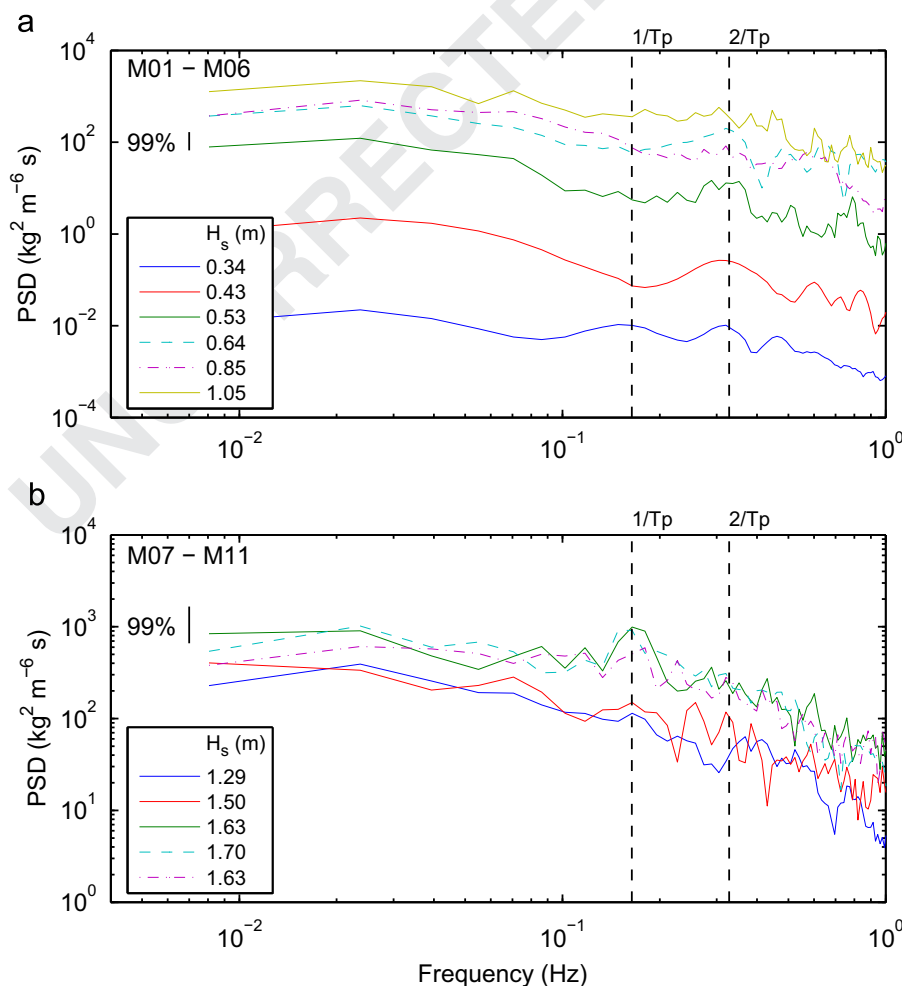


Fig. 7. The power spectral density, PSD, of 4 Hz suspended sediment concentration, SSC, from the ABS 0.01 m above the bed, with the 99% confidence interval shown. (a) shows SSC results from M01 to M06 when 2D or q-2D ripples populated the bed, and (b) shows results from M07 to M11 when the bed was 3D rippled or hummocky. The vertical dashed lines show the peak spectral wave and half-wave frequencies,  $1/T_p$  and  $2/T_p$ , respectively. Note the difference in the scale of the vertical axis in (a) and (b).

frequency bands of the single-sided spectra 64 degrees of freedom. The 99% confidence interval was calculated using the chi-square approach. Fig. 7 shows the PSD of the 4 Hz SSC 0.01 m above the bed for experiments M01–M11. The grouping in Fig. 7 is in accordance with the emergence of different plan-form bedform geometries during the experimental sequence, and enables the differences in the frequency distribution of sediment entrainment above two distinct bedform types to be examined. During M01–M06 the ripples had 2D or q-2D plan-form geometries and the PSDs of the SSCs from these experiments are shown in Fig. 7(a). Fig. 7(b) shows the results from M07 to M11 during which the bed was dominated by 3D ripples or hummocks. The dashed vertical lines indicate the frequencies of the peak spectral wave period,  $1/T_p$ , and the half-wave period,  $1/2T_p$ . For each experiment, there is seen to be a broad spectral zone in the PSD between approximately 0.01 and 0.1 Hz, peaking about 0.02 Hz. This trend is deemed to be associated with the wave groups that tended to occur between 20 and 60 s.

For experiments M02–M05, the broad low frequency peak is larger than the higher frequency fluctuations by more than the 99% confidence interval, indicating that it is a wave group signature and that, therefore, wave groups play a significant role in the suspension of sediment.

At higher frequencies, there are a number of peaks in the PSDs, some of which are greater than the 99% confidence interval shown. In Fig. 7(a), these statistically significant peaks are around twice the peak spectral wave frequency, and are consistent through M01–M05. There is much less of a structure to the PSDs

shown in Fig. 7(b). Those few statistically significant high frequency peaks tend to occur at the wave frequency.

There is a notable difference in structure of the spectra shown in Fig. 7(a) and (b). When  $H_s$  was less than 1.0 m the bed was dominated by 2D or q-2D ripples, and the intra-wave suspension of sediment at half the wave frequency dominated the near bed PSD of SSC. At stronger wave forcing,  $H_s > 1.0$  m, this  $2/T_p$  intra-wave structure in the SSC no longer appears to be present, and in some cases there is a  $1/T_p$  intra-wave structure. This breaking down of the  $2/T_p$  intra-wave structure is likely to be for two reasons: (i) the stronger wave forcing meant that much more sediment was continually in suspension making the intra-wave fluctuations less discernible, and (ii) the larger bedform wavelengths made it more likely that only one suspension event per wave cycle was detected by the ABS.

### 3.3. Variations in SSC time scales with height above a rippled bed

Fig. 8 shows the PSD of the SSC at seven heights above the bed between 0.01 and 0.50 m from M04 where  $H_s = 0.64$  m and the bed was dominated by steep-sided 2D ripples. As in Fig. 7, there is a broad low frequency plateau deemed to be associated with wave groups, and a number of smaller peaks at higher frequencies. Close to the bed,  $z \leq 0.10$  m, there are statistically significant peaks at twice the peak spectral wave frequency,  $1/2T_p$ , which are most likely associated with the entrainment of sediment-laden vortices within the WBL. At  $z = 0.01$  m, this peak is quite clear,

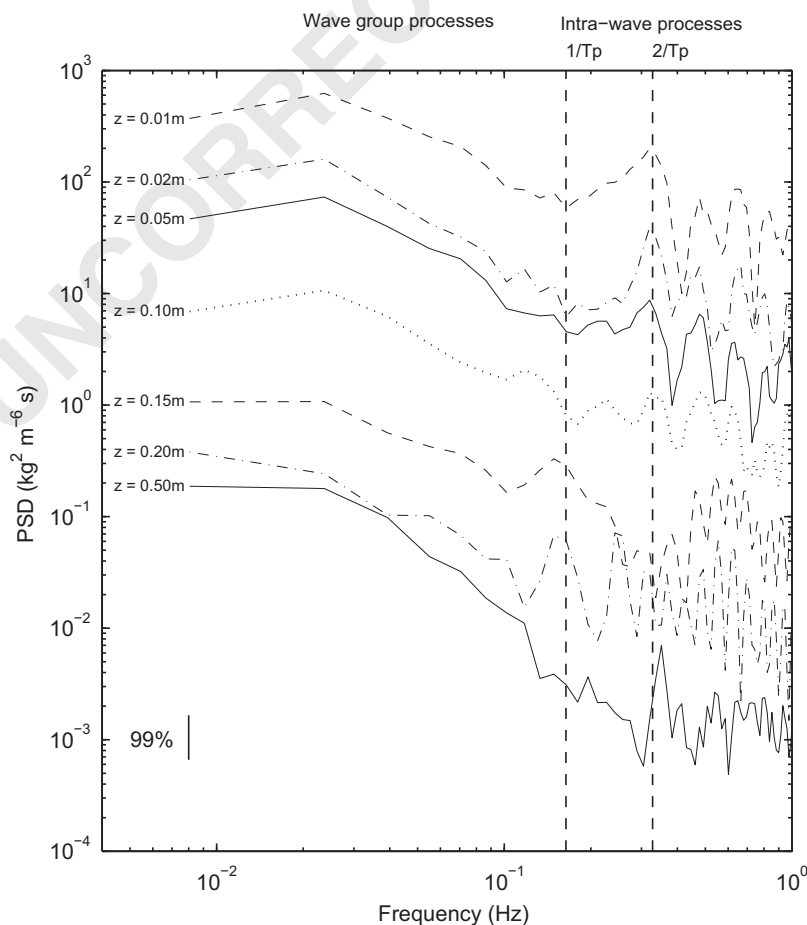


Fig. 8. The power spectral density, PSD, of 4 Hz suspended sediment concentration, SSC, at different heights,  $z$ , above the bed from M04. The vertical dashed lines show the peak spectral wave and half-wave frequencies,  $1/T_p$  and  $2/T_p$ , respectively.

indicating that there was a strong vortex shedding influence within the WBL. At higher elevations, the magnitude of the high frequency peaks relative to the low frequency plateau diminishes somewhat, but is still statistically significant up to  $z=0.10$  m. For  $0.15 \leq z \leq 0.2$  m there are statistically significant peaks at the peak spectral wave frequency. The sediment above the WBL was likely to be a combination of sediment entrained locally and advected from adjacent ripples. For  $z=0.5$  m there is a significant broad low frequency zone around  $\sim 0.02$  Hz, suggesting that only during the passage of wave groups was sediment pumped to these higher free stream elevations, as shown in Fig. 5.

#### 3.4. Instantaneous SSC above an evolving bed

Fig. 9 shows 3 min time series of 4 Hz SSC at 1 Hz up to 0.5 m above the bed for five experiments with increasing wave forcing and different bedform conditions. The experiments shown are

(a) M02, (b) M04, (c) M06, (d) M08 and (e) M11 where  $H_s$  ranged from 0.43 to 1.63 m and the bedforms were (a) 2D ripples of low steepness, (b) steep-sided 2D ripples, (c) q-2D ripples, (d) 3D ripples and (e) hummocks. The horizontal velocity time series from the ADV, and  $\delta_w$ , are also shown in Fig. 9. The timings of the waves and wave groups were closely synchronised through these five experiments. In terms of orbital velocities, the only major difference between each experiment was the orbital velocity amplitude of each wave, as the sequence of wave periods remained consistent throughout the experiments. Fig. 9(a) shows the results from M02 when  $H_s=0.43$  m and small 2D ripples of low steepness were present on the bed. In this case there was little sediment entrainment in the majority of wave cycles, with only the orbital velocity amplitudes of the larger waves being sufficient to entrain sediment. There are two wave groups inducing significant wave pumping shown in Fig. 9(a), with the maximum orbital velocities occurring at approximately 60 and 130 s. During each of these wave groups the near bed,  $z < 0.1$  m,

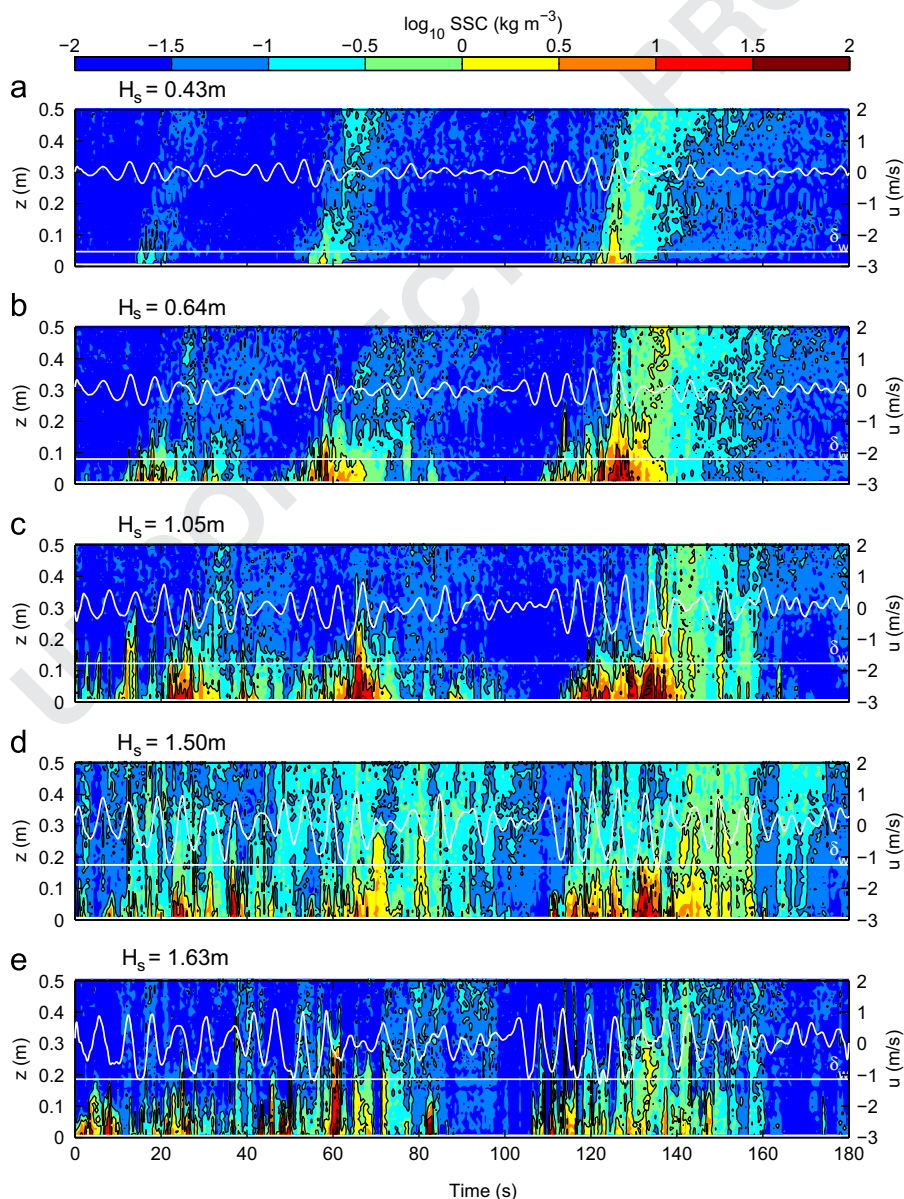


Fig. 9. Time series of 4 Hz suspended sediment concentration (SSC) at 1 Hz up to 0.5 m above the bed from (a) M02, (b) M04, (c) M06, (d) M08 and (e) M11 during which the significant wave height,  $H_s$ , and bedform conditions differed. The height above the bed,  $z$ , is indicated on the left. The horizontal velocity time series are shown in white with the velocity,  $u$ , scale on the right. The temporally averaged wave boundary layer thickness,  $\delta_w$ , are indicated by the horizontal white lines.



SSC peaked after the largest orbital velocities. During these wave groups the wave pumping caused inversions of the SSC profile after the passage of each wave group, with the SSC being higher in the free stream than the WBL at approximately 70 and 140 s. During these SSC profile inversions the SSC was greater than  $0.1 \text{ kg m}^{-3}$  at  $z=0.5 \text{ m}$  and approximately  $0.01 \text{ kg m}^{-3}$  at  $z=0.05 \text{ m}$ . When  $H_s=0.64 \text{ m}$  and steep-sided ripples were present on the bed, there was a similar underlying structure to the SSC field, as shown in Fig. 9(b), with sediment pumping starting at approximately 60 and 130 s. There was also some sediment pumping due to a shorter duration wave group starting at the beginning of the time series shown. Compared with Fig. 9(a), Fig. 9(b) shows increased intermittent sediment entrainment outside the dominant wave groups associated with vortices (O'Hara Murray et al., 2011). The results in Fig. 9(c) are from M06 when  $H_s=1.05 \text{ m}$  and when steep-sided q-2D ripples dominated the bed. Fig. 9(c) shows enhanced sediment entrainment during the three dominant wave groups and sediment entrainment at intra-wave frequencies, typically confined to  $z < 0.25 \text{ m}$ , occurring during most wave cycles. The repeated intra-wave sediment entrainment occurred because the orbital diameter was greater than the ripple wavelength for most wave cycles in this experiment (O'Hara Murray et al., 2011). In Fig. 9(d), which shows results from when  $H_s=1.50 \text{ m}$  and when 3D ripples dominated the bed, the SSC at  $0.3 < z < 0.5 \text{ m}$  was greater than  $0.1 \text{ kg m}^{-3}$  during most of the 3 min time series. The SSC at  $z=0.05 \text{ m}$  was lower under the larger waves in Fig. 9(d), than in Fig. 9(c) when  $H_s=1.05 \text{ m}$ . This reduction in the SSC within the

WBL is related to the reduction in the steepness of the ripple faces. The faces of the 3D ripples in M08 were less steep than the q-2D ripples in M06 which encouraged flow separation and enhanced turbulence production within the WBL. Finally, Fig. 9(e) shows the SSC field when  $H_s=1.63 \text{ m}$  and hummocks with wavelengths of  $0.75 \text{ m}$  populated the bed. During the 180 s time series shown, the SSC was generally lower when  $H_s=1.63 \text{ m}$  than when  $H_s=1.50 \text{ m}$ . This was considered to be due to the transition from 3D ripples to hummocks, possibly reducing turbulence production and coherent vortex formation and shedding.

### 3.5. Wave cycle-mean SSC profiles through a wave group

Fig. 10 shows the wave cycle mean SSC profiles through a wave group during M05 where  $H_s=0.85 \text{ m}$  and the bed was dominated by q-2D ripples. The upper panel shows the horizontal velocity time series with the wave cycles defined to start at the zero-up crossings (offshore-onshore flow reversal). The lower panels show the corresponding wave cycle-mean SSC profile (solid lines), for each wave, and the wave group mean profile (dashed lines). The wave cycle-mean SSC profile changed shape during the passage of the wave group, broadly in accordance with changes observed by Villard et al. (2000). This was due to (i) enhanced intra-wave suspension during the larger waves and (ii) wave pumping effects. During the first two waves, the SSC was lower than the wave group mean at all heights above the bed. It is under the larger third and fourth waves that the SSC close to the bed approached and exceeded the wave group mean

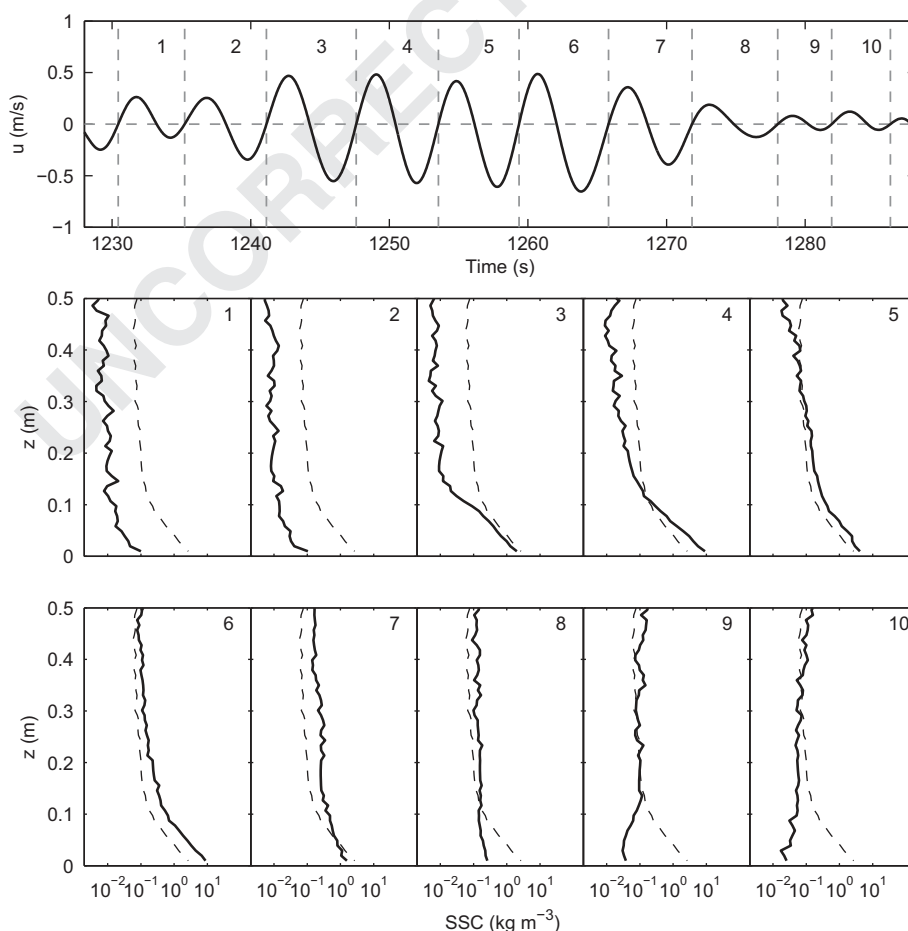


**Fig. 10.** Wave cycle mean suspended sediment concentration, SSC, profiles from M05 through a wave group. The upper panel shows the horizontal velocity time series from the ADV with each wave cycle numbered (1–10). The lower panels show the wave cycle mean SSC profiles for each wave (solid lines) and the wave group mean SSC profile (dashed lines). The numbering of the lower panels corresponds to the numbering of the waves in the upper panel.

concentration. This near bed concentration remained high during the four largest waves and only began to fall below the wave group mean concentration during the seventh, smaller, wave. In the free stream there was a delayed response, with the SSC approaching the wave group mean SSC during wave five. During the final two cycles in the wave group, the SSC was generally higher in the free stream than the WBL. This SSC profile inversion was due to the sediment, pumped up during the passage of the wave group, remaining in suspension while there was little intra-wave sediment entrainment under the final small waves. Under the four largest waves, waves 3–6, the decay of sediment concentration with height was approximately exponential up to  $\sim 0.13$  m, about 4.5 times the ripple height. The height to which time average SSC profiles are exponential is typically three to four times the ripple height (Van Rijn, 1993; Van der Werf et al., 2006; Thorne et al., 2009). This region of exponential decay is closely related to the upward propagation of vortices and the wave boundary layer thickness. This thickness of this near bed region is larger, at  $\sim 4.5\eta$ , during the largest waves in the group than during the measurement burst on average, which was  $\sim 3\eta$ . The thickness of these regions of exponential decay agree with the estimates of the wave boundary layer thickness made in Section 2.3, listed in Table 1. Eq. (7) was fitted to the wave cycle-mean SSC profiles in this near bed region, and the rate of near bed exponential decay was roughly constant during waves 3–6, with  $L = 0.03$ – $0.06$  m. These decay rates are similar to those of the time-mean profiles above 2D and q-2D ripples shown in Fig. 4.

Fig. 10 shows cycle-mean profiles through a wave group above steep-sided 2D ripples. The time-mean SSC profiles from M04 and M06, shown in Fig. 4 by (○) and (+), resemble the cycle-mean profiles in Fig. 10(b) under the largest four waves, 3–6. This is not only because of the common bedform conditions, but also because during these waves there was substantial intra-wave sediment entrainment that dominated the contribution to the time average SSC profiles. The cycle-mean concentrations during the smaller waves also contributed to the total time average SSC, but mainly at elevations of  $z > 0.2$  m, in the free stream, where the SSC was maintained by wave pumping.

#### 4. Discussion

Time series of SSC have been examined up to 0.8 m above an evolving medium-grained sandy bed. The order of bedform development as the significant wave height was incremented was 2D ripples, q-2D ripples, 3D ripples and hummocks. Whilst the suspension of sediment occurred at a variety of different time scales, a common feature across all the experiments was increased sediment suspension during the passage of wave groups. This observation is in accordance with the previous studies both in wave flumes (Villard et al., 2000; Vincent and Hanes, 2002; Williams and Bell, 2006) and in the field (Hanes, 1991; Osborne and Greenwood, 1993; Hay and Bowen, 1994a, 1994b). The existence of high SSC at low wave group frequencies is broadly shown by examining the SSC in the frequency domain, but is much more evident in the time domain. Whilst wave groups appear to be important, especially at higher elevations, processes acting at higher, intra-wave, frequencies play a fundamentally important role in the initial resuspension of sediment within the WBL. This too can be seen in the time domain, but can clearly be shown by examining the time series of SSC in the frequency domain, as shown by Figs. 7 and 8.

##### 4.1. Near bed intra-wave sediment suspension processes over an evolving bed

The largest orbital velocities occurred during the passage of wave groups, and it is these high near bed velocities that are

mainly associated with intra-wave sediment entrainment. For example, vortex entrainment occurs above steep ripples when the orbital diameter is between one and four times the ripple wavelength (Malarkey and Davies, 2002; O'Hara Murray et al., 2011). These higher than average orbital velocities during wave groups caused, therefore, the peaks in the PSD of near bed SSC at wave group frequencies. There were, however, also peaks in the PSD of near bed SSC at higher, intra-wave, frequencies. There is a striking difference in the frequency of these intermittent intra-wave suspensions above (i) the 2D ripples and (ii) the 3D ripples and hummocks. Above the 2D ripples, the intra-wave suspension process occurred twice in the wave cycle and is associated with the advection of sediment-laden vortices over ripple crests around flow reversal (Nakato et al., 1977; Sleath and Wallbridge, 2002; Davies and Thorne, 2005; Van der Werf et al., 2007). Such intra-wave suspensions depend heavily on the orbital velocity and are intermittent under irregular waves (O'Hara Murray et al., 2011). Thus, the peaks at intra-wave frequencies in Fig. 7(a) have lower magnitudes than the broad peaks at wave group frequencies.

Above the 3D ripples and hummocks, the entrainment of sediment at intra-wave frequencies was not as discernible as it was over the 2D, and q-2D, ripples. This is most likely due to high SSC levels being maintained throughout most wave cycles. These high SSC levels were likely to be maintained through the wave cycle by the strong orbital velocities, but also by the local advection of vortices at flow reversal and the transport of sand from other points on the mega-ripple profile. Hay and Bowen (1994a) observed similar merging of suspended sediment structures in field data and Vincent et al. (1999) observed similar sediment entrainment patterns above mega-ripples.

##### 4.2. The importance of considering wave group character

The entrainment of sediment high into the free stream under wave groups has implications in terms of the horizontal advection of sediment by waves and currents. This is because sediment entrained in the free stream is more susceptible to horizontal transport, due to wave asymmetry or currents, for example, than the sediments within the bottom boundary layer. A consideration

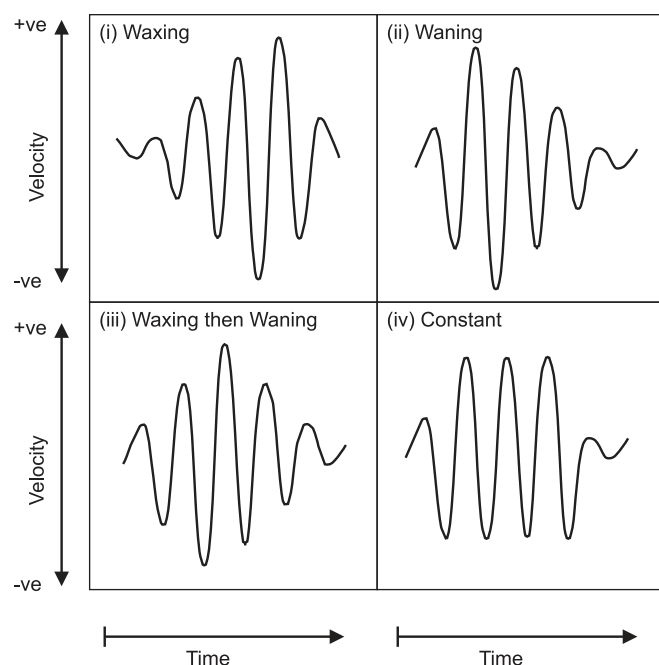
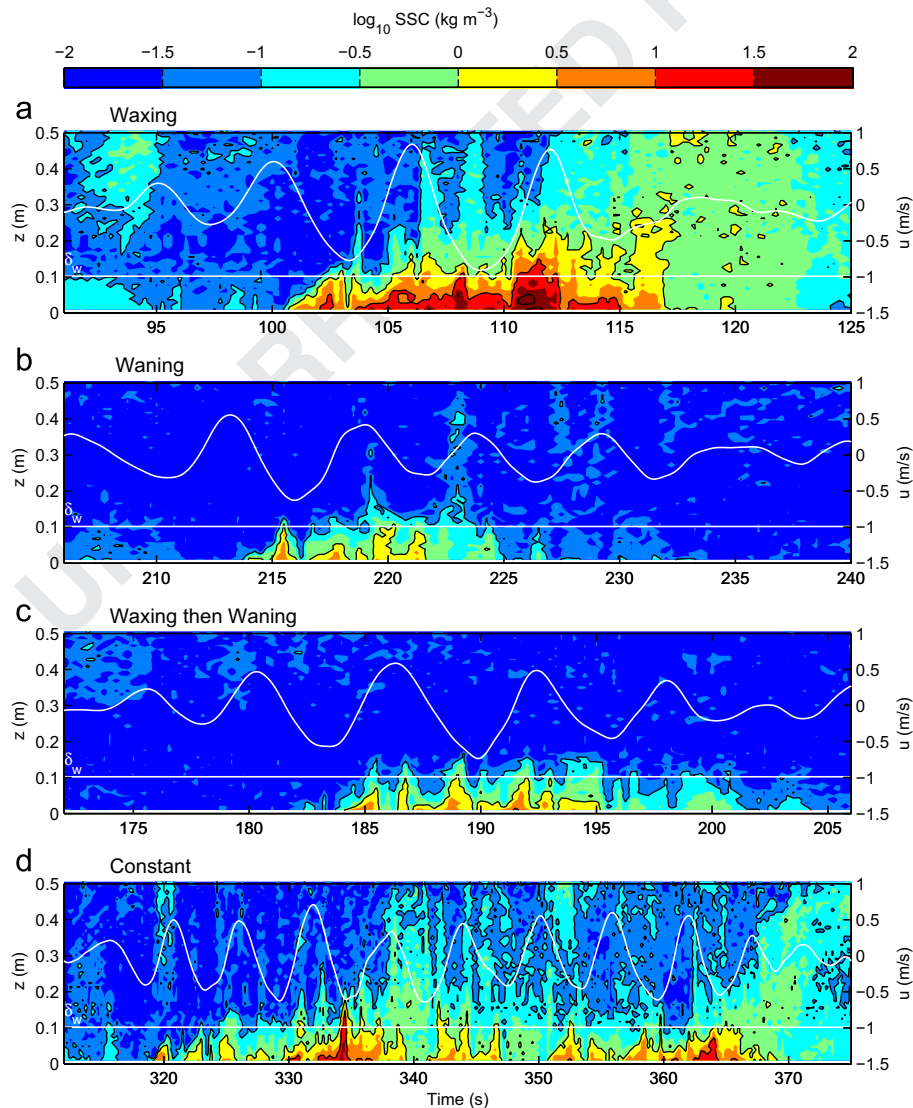


Fig. 11. Schematic diagram of four wave group types.

of the range and types of wave group characteristics may refine sediment transport models and the experimental design of field data collection. Four broad types of wave groups are depicted in Fig. 11: (i) waxing (increasing velocity amplitudes), (ii) waning (decreasing velocity amplitudes), (iii) waxing then waning (increasing then decreasing velocity amplitudes) and (iv) constant (short-term regular above average velocity amplitudes). Another important variable in the character of wave groups is the number of waves in a group. The type of wave group, and the number of waves in a group, could have a significant impact on the height and concentration of suspended sediment. One simple hypothesis is that a waxing wave group would pump more sediment higher above the bed than a waning wave group with the same number of waves. Another hypothesis considering two waxing wave groups with different numbers of waves is that more sediment would be pumped higher under the group with more waves.

To start to test these hypotheses of wave group character, wave groups that conform to the four types, outlined in Fig. 12, were identified in the ADV velocity time series. Fig. 12 shows the 4 Hz SSC time series during these four wave groups from M05 where  $H_s=0.85$  m and the bed was populated by q-2D vortex shedding ripples. The wave groups identified all occurred during a

5 min period of time, while the ABS was above the mid-point between the crest and trough of a ripple. There are a number of factors that make this comparison difficult including (i) the difference in wave characteristics, including velocity amplitudes, across each type of group and (ii) the difference in length of each group. The wave groups were chosen in order to minimise such complications. For example, in Fig. 12(a)–(c) the length of the time series shown is 34 s. The group of approximately constant wave heights shown in Fig. 12(d) is, however, 63 s in duration. Despite these differences there are some general observations that can be made. The highest, and most prolonged, concentration of suspended sediment above  $z \sim 0.2$  m occurred at the end of the waxing wave group shown in Fig. 12(a) between 117 and 123 s. During this time the orbital velocity was relatively small, and yet the SSC is greater than  $0.3 \text{ kg m}^{-3}$  ( $\log_{10} \text{SSC} > -0.5$ ) throughout all of the 0.5 m vertical region shown. This is most likely to be the settling out of sediment pumped up during the wave group. There is also, however, a suggestion of high concentrations of sediment being picked up, at  $\sim 117$  s, despite a fall in velocity at the same time. Similar upward 'bursts' of sediment, occurring when a wave group is terminated by a sudden reduction in the orbital velocity amplitude, were observed by Villard et al. (2000) and Vincent and



**Fig. 12.** Examples of suspended sediment concentration, SSC, time series under wave groups that broadly conform to four different types illustrated in Figure 11: (a) waxing, (b) waning, (c) waxing then waning and (d) constant. The height above the bed,  $z$ , is indicated on the left and the horizontal velocity time series are shown in white with the velocity,  $u$ , scale on the right. The temporally averaged wave boundary layer thickness,  $\delta_w = 0.102$  m, is shown by the white horizontal line in each case.

Hanes (2002). There is no evidence of high SSC after the wave groups shown in Fig. 12(b) and (c), either settling out or being entrained through upward 'bursts'. This is because these wave groups were not as effective at pumping sediment to high elevations, as the waxing wave group, but also because they were not terminated by a sudden reduction in the velocity amplitude.

Fig. 12(d) shows evidence for two vertical advection events. The first is under the fifth oscillation,  $\sim 340$  s, which is marginally smaller in amplitude than the other oscillations, and the second is at the end of the group under the smaller velocity amplitudes. The first vertical 'burst', at  $\sim 340$  s, was relatively short lived and is likely to be associated with the high SSC entrained during the previous cycle. During the second 'burst', at the end of the wave group in Fig. 12(d), there was a time lag of two cycles between entrainment at the bed and relatively high SSC at  $z \sim 0.4$  m, typical of the wave pumping effect. This pumping of sediment continuing at the end of the group is similar to the upward 'bursts' of sediment observed Villard et al. (2000) and Vincent and Hanes (2002) following sudden reductions in the orbital velocity, but could also be due to the finer grains still being supported and there still being adequate vertical turbulence to maintain pumping.

#### 4.3. Regular and irregular waves

Irregular wave sequences are often parameterised by single equivalent regular waves. For example, in this paper the significant wave heights and peak spectral wave periods were presented, along with the Shields parameters based on the significant wave orbital velocities. This work suggests that sediment suspensions are strongly dependent on the character of the irregular waves, and not necessarily just on the bedforms present and the significant wave forcing conditions during the measurement burst. The examination of the wave cycle-mean SSC profiles through a wave group in Section 3.5 showed that the SSC profiles that most resembled the burst average profiles presented in Section 2.4.1 were those under the highest waves in the group. These suspensions, where the wave boundary layer thickness, and vertical extent of mixing, were at a maximum, therefore dominated the near bed time-mean concentration profiles. This lends some support to the concept of using significant wave heights, or orbital velocities, as parameters describing irregular waves in sediment transport formulations. However, Vincent et al. (2001) reported on the SISTEX99 experiment conducted in a large wave flume with both regular and irregular waves, and found that suspensions were generally higher under regular waves than under irregular waves with a similar significant wave height. One explanation for this is that wave pumping occurs under wave groups and regular waves are essentially a continuous group of waves with constant amplitude and phase, most like type (iv) identified in Section 4.2. Thus, continuous wave pumping occurs under regular waves. Vincent and Hanes (2002) also reported on the SISTEX99 experiment and observed the SSC in the free stream reaching a state of equilibrium where the continuous generation and vertical advection of turbulence was enough to continually maintain a high SSC. This phenomenon was also noted by O'Hara Murray (2011) in a comparison of sediment suspensions under regular and irregular waves. Under the irregular waves, the wave pumping effect is intermittent and only occurs under wave groups with orbital velocities large enough for substantial entrainment.

It is not just the hydrodynamics that need to be considered when comparing regular and irregular waves. Under regular waves, the bedforms are in constant equilibrium with the flow, making the influence from the bed over the SSC constant, along with the wave forcing. Under irregular waves, the bed takes longer to reach equilibrium (Marsh et al., 1999), but is also likely to be much more dynamic, with ripple crests being eroded under the larger waves, for

example. Vincent et al. (1991) and Vincent and Hanes (2002) noted how the possible variation in ripple geometry through a wave group might contribute to the intra-wave suspension of sediment. Thus, future comparisons should consider time series of parameters, such as the Shields parameter, taking into account both the flow and bed conditions, at a wave or intra-wave time scale.

## 5. Conclusions

This work examines sediment suspensions within the bottom 0.8 m over a range of bedforms and irregular wave forcing conditions. High resolution ABS was used in order to resolve intra-wave processes close to the bed, but also monitor SSC levels in the free stream. In both the WBL and the free stream, the SSC responded to fluctuation in orbital velocity at wave group frequencies. The higher velocities during wave groups generated increased levels of turbulence, enhancing vortex formation and shedding. It is, therefore, intra-wave sediment suspension processes that are important in the initial entrainment of sediment within the WBL, especially when coherent vortices are generated, as is the case above steep ripples. In the free stream, the dominant control over the SSC was wave groups and the wave pumping effect. Time lags of 2–3 wave cycles were observed between initial sediment entrainment at the bed and peak SSC at  $z > 0.5$  m above the bed.

The high SSC in the WBL due to intra-wave entrainment is arguably the most important process to consider when calculating net suspended sediment transport (Van der Werf et al., 2006). However, it is also important to consider the entrainment of sediment to higher free stream elevations under wave groups. The wave pumping effect enables sediment to be entrained to higher elevations than by intra-wave processes alone. Once at these high elevations the suspended sediments can remain in suspension for a number of wave periods, depending on its settling velocity and the turbulence generation. This substantially increased suspension time could lead to increased cross-shore or long-shore transport, especially in the presence of currents. It is also thought that the wave pumping effect is a mechanism by which sediment can be entrained to elevations unobtainable under individual waves of similar characteristics.

Wave groups are characteristic of irregular wave forcing, which is typical in the field. The simultaneous measurements of water velocity, bedforms and SSC presented here were made in a large scale flume facility, offering some reduction in the complexity of the natural world. However, much more refined experiments are recommended to further examine the importance of irregular waves, and wave group character, on the SSC. Specifically, experiments with a strong control over the character of wave groups are recommended in order to ensure that when comparing groups with different characters, the group length and highest wave in the group are, for example, the same. It would also be beneficial to compare the velocity and SSC frequency spectra resulting from a highly ordered, and repeated, irregular wave spectrum. Such a wave spectrum might have a clear narrow peak around the significant wave height, but also a very clear peak corresponding to wave groups. This would greatly aid the identification of peaks in the SSC spectrum at these two distinct frequencies. Finally, there is scope for experiments comparing regular with irregular wave forcing to be designed. The outcome of such detailed studies is important to inform numerical modelling, and to refine the design of field experiments.

## Acknowledgments

This work was supported by the European Union, through its access to large-scale facilities, and by the Natural Environment



Research Council and the University of Liverpool for PhD funding. The authors thank Prof. J.J. Williams at Associated British Ports, who coordinated the Deltaflume experiments and Dr. Paul S. Bell and Dr. Benjamin D. Moate at the National Oceanography Centre for many usefully discussions regarding the analysis of the acoustic data. We would also like to thank Prof. Stephen S. Flint at the School of Environmental Sciences, University of Liverpool, for his support, and Dr. Jaco H. Baas, Bangor University, and Prof. Andy J. Plater, University of Liverpool, for examining the PhD thesis from which this work is taken. Finally, we would like to thank the guest editor, Prof. A.E. Hay, and the two reviewers for their constructive comments that improved the manuscript.

## References

Bell, P.S., Williams, J.J., 2002. Comprehensive Measurements of Sediment Resuspension Processes by Waves at Full-Scale. POL Internal Document No. 143. Technical Report, Proudman Oceanographic Laboratory.

Bosman, J.J., van der Velden, E.T.J.M., Hulsbergen, C.H., 1987. Sediment concentration measurement by transverse suction. *Coastal Engineering* 11 (4), 353–370.

Carter, D.J.T., 1982. Prediction of wave height and period for a constant wind velocity using the JONSWAP results. *Ocean Engineering* 9 (1), 17–33.

Clarke, T., Lesht, B., Young, R., Swift, D., Freeland, G., 1982. Sediment resuspension by surface-wave action: an examination of possible mechanisms. *Marine Geology* 49 (1–2), 43–59. URL <<http://www.sciencedirect.com/science/article/pii/0025322782900287>>.

Davies, A.G., Thorne, P.D., 2005. Modelling and measurement of sediment transport by waves in the vortex ripple regime. *Journal of Geophysical Research* 110 (C05017).

Davies, A.G., Thorne, P.D., 2008. Advances in the study of moving sediments and evolving seabeds. *Surveys in Geophysics* 29 (1), 1–36.

Davies, A.G., Villaret, C., 1999. Eulerian drift induced by progressive waves above rippled and very rough beds. *Journal of Geophysical Research—Oceans* 104 (C1), 1465–1488.

Doucette, J.S., O'Donoghue, T., 2006. Response of sand ripples to change in oscillatory flow. *Sedimentology* 53 (3), 581–596.

Emery, W.J., Thompson, R.E., 1997. *Data Analysis Methods in Physical Oceanography*. Elsevier Science.

Goring, D.G., Nikora, V.I., 2002. Despiking acoustic Doppler velocimeter data. *Journal of Hydraulic Engineering—ASCE* 128 (1), 117–126.

Grasmeijer, B.T., Kleinhans, M.G., 2004. Observed and predicted bed forms and their effect on suspended sand concentrations. *Coastal Engineering* 51 (5–6), 351–371.

Green, M.O., Black, K.P., 1999. Suspended-sediment reference concentration under waves: field observations and critical analysis of two predictive models. *Coastal Engineering* 38 (3), 115–141.

Hanes, D.M., 1991. Suspension of sand due to wave groups. *Journal of Geophysical Research—Oceans* 96 (C5), 8911–8915.

Hansen, E.A., Fredsoe, J., Deigaard, R., 1994. Distribution of suspended sediment over wave-generated ripples. *Journal of Waterway Port Coastal and Ocean Engineering—ASCE* 120 (1), 37–55.

Hay, A.E., Bowen, A.J., 1994a. Coherence scales of wave-induced suspended sand concentration fluctuations. *Journal of Geophysical Research* 99 (C6), 12749–12765. doi:10.1029/94JC00290.

Hay, A.E., Bowen, A.J., 1994b. Space-time variability of sediment suspension in the nearshore zone. In: *Coastal Dynamics'94*, pp. 962–975.

Larsen, L.H., 1982. A new mechanism for seaward dispersion of midshelf sediments. *Sedimentology* 29 (2), 279–283.

Malarkey, J., Davies, A.G., 2002. Discrete vortex modelling of oscillatory flow over ripples. *Applied Ocean Research* 24 (3), 127–145.

Marsh, S.W., Vincent, C.E., Osborne, P.D., 1999. Bedforms in a laboratory wave flume: an evaluation of predictive models for bedform wavelengths. *Journal of Coastal Research* 15 (3), 624–634.

Nakato, T., Locher, F.A., Glover, J.R., Kennedy, J.F., 1977. Wave entrainment of sediment from rippled beds. *Journal of the Waterway Port Coastal and Ocean Division—ASCE* 103 (1), 83–99.

Nielsen, P., 1992. *Coastal Bottom Boundary Layers and Sediment Transport*. World Scientific.

O'Hara Murray, R.B., 2011. *Suspended Sand Concentrations and Bedform Evolution Under Irregular Waves*. Ph.D. Thesis, The University of Liverpool.

O'Hara Murray, R.B., Thorne, P.D., Hodgson, D.M., 2011. Intrawave observations of sediment entrainment processes above sand ripples under irregular waves. *Journal of Geophysical Research—Oceans* 116 (C01001).

Osborne, P.D., Greenwood, B., 1993. Sediment suspension under waves and currents—time scales and vertical structure. *Sedimentology* 40 (4), 599–622.

Osborne, P.D., Vincent, C.E., 1996. Vertical and horizontal structure of suspended sand concentrations and wave-induced fluxes over bedforms. *Marine Geology* 131 (3–4), 195–208.

Pedocchi, F., Garcia, M.H., 2009. Ripple morphology under oscillatory flow: 1. Prediction. *Journal of Geophysical Research—Oceans* 114, 16.

Ribberink, J.S., Al-Salem, A.A., 1994. Sediment transport in oscillatory boundary layers in cases of rippled beds and sheet flow. *Journal of Geophysical Research* 99 (C6), 12707–12728.

Shi, N.C., Larsen, L.H., 1984. Reverse sediment transport induced by amplitude-modulated waves. *Marine Geology* 54 (3–4), 181–200.

Sleath, J.F.A., Wallbridge, S., 2002. Pickup from rippled beds in oscillatory flow. *Journal of Waterway, Port, Coastal, and Ocean Engineering* 128 (6), 228–237.

Soulsby, R.L., 1997. *Dynamics of Marine Sands. A Manual for Practical Applications*. HR Wallingford.

Thorne, P.D., Davies, A.G., Bell, P.S., 2009. Observations and analysis of sediment diffusivity profiles over sandy rippled beds under waves. *Journal of Geophysical Research—Oceans* 114, 16.

Thorne, P.D., Hanes, D.M., 2002. A review of acoustic measurement of small-scale sediment processes. *Continental Shelf Research* 22 (4), 603–632.

Thorne, P.D., Hardcastle, P.J., Soulsby, R.L., 1993. Analysis of acoustic measurements of suspended sediments. *Journal of Geophysical Research—Oceans* 98 (C1), 899–910.

Van der Werf, J.J., Doucette, J.S., O'Donoghue, T., Ribberink, J.S., 2007. Detailed measurements of velocities and suspended sand concentrations over full-scale ripples in regular oscillatory flow. *Journal of Geophysical Research—Earth Surface* 112 (F2).

Van der Werf, J.J., Ribberink, J.S., O'Donoghue, T., Doucette, J.S., 2006. Modelling and measurement of sand transport processes over full-scale ripples in oscillatory flow. *Coastal Engineering* 53 (8), 657–673.

Van Rijn, L.C., 1993. *Principles of Sediment Transport in Rivers, Estuaries and Coastal Seas*. Aqua Publications.

Villard, P.V., Osborne, P.D., 2002. Visualization of wave-induced suspension patterns over two-dimensional bedforms. *Sedimentology* 49 (2), 363–378.

Villard, P.V., Osborne, P.D., Vincent, C.E., 2000. Influence of wave groups on SSC patterns over vortex ripples. *Continental Shelf Research* 20 (17), 2391–2410.

Vincent, C., Hanes, D., Bowen, A., 1991. Acoustic measurements of suspended sand on the shoreface and the control of concentration by bed roughness. *Marine Geology* 96 (1–2), 1–18.

Vincent, C., Young, R.A., Swift, D.J.P., 1982. On the relationship between bedload and suspended sand transport on the inner shelf, Long Island, New York. *Journal of Geophysical Research* 87, 4163–4170.

Vincent, C.E., Hanes, D.M., 2002. The accumulation and decay of near-bed suspended sand concentration due to waves and wave groups. *Continental Shelf Research* 22 (14), 1987–2000.

Vincent, C.E., Hanes, D.M., Dohmen-Janssen, C.M., Klopman, G., McLean, S.R., Obhrai, C., Ribberink, J.S., 2001. Suspension by regular and group waves over bedforms in a large wave flume (SISTEX99). In: *Coastal Dynamics'01*, pp. 303–312.

Vincent, C.E., Marsh, S.W., Webb, M.P., Osborne, P.D., 1999. Spatial and temporal structures of suspension and transport over megaripples on the shore face. *Journal of Geophysical Research—Oceans* 104 (C5), 11215–11224.

Vincent, C.E., Osborne, P.D., 1993. Bedform dimensions and migration rates under shoaling and breaking waves. *Continental Shelf Research* 13 (11), 1267–1280.

Wiberg, P.L., Sherwood, C.R., 2008. Calculating wave-generated bottom orbital velocities from surface-wave parameters. *Computers and Geosciences* 34 (10), 1243–1262.

Williams, J., Rose, C., Thorne, P., 2002. Role of wave groups in resuspension of sandy sediments. *Marine Geology* 183 (1–4), 17–29.

Williams, J.J., Bell, P.S., 2006. Laboratory investigation of bedform dynamics and resuspension of sandy sediments at field scale. *Journal of Coastal Research* 2, 810–815.